Research Article

Journal of Environmental Nanotechnology

# Sustainable Treatment of Metronidazole-contaminated Wastewater via Integrated Adsorption and UV-assisted Degradation Using ZnO-modified Rice Husk Biochar and Silica–gelatin Composites

Suriya Shaffi Bhat[1], P. Rajasekaran[2], M. Sathya[3], D. Boovitha[4], L. Ganeshbabu[5*] and R. Girimurugan[6]

[1]Department of Civil Engineering, Faculty of Engineering, Tishk International University, Erbil, Iraq
[2]Department of Mechanical Engineering, Er. Perumal Manimekalai College of Engineering, Hosur, TN, India
[3]Department of Chemistry, Erode Arts and Science College, Erode, TN, India
[4]Department of Computer Science and Engineering, Nandha College of Technology, Perundurai, TN, India
[5]Department of Robotics and Automation, Easwari Engineering College, Chennai, TN, India
[6]Department of Mechanical Engineering, Nandha College of Technology, Perundurai, TN, India
Received: 20.06.2026 Accepted: 22.07.2026 Published: 30.09.2026
*ganeshbabume8@gmail.com

## ABSTRACT

This study developed ZnO-functionalized rice-husk biochar (RHB–ZnO) and a silica-reinforced gelatin composite (Gel–$SiO_2$) for the adsorption and UV-assisted removal of metronidazole (MET) from water. The composites were characterized using XRD, FTIR, and BET analyses and evaluated at MET concentrations of 0.1–10 mg $L^{-1}$ under 254-nm UV irradiation. Although biochar- and biopolymer-based materials have been investigated separately, their comparative adsorption, UV-assisted removal, mineralization, and long-term reusability toward pharmaceutical contaminants remain insufficiently understood. The novelty of this work lies in the direct evaluation of these two sustainable composite systems under identical treatment conditions over 15 reuse cycles. BET analysis showed that ZnO functionalization increased the specific surface area of rice-husk biochar from 546.32 to 564.22 $m^2$ $g^{-1}$, while XRD confirmed the formation of crystalline ZnO within the predominantly amorphous biochar matrix. Among the studied systems, the UV/Gel–$SiO_2$ composite exhibited approximately 94.5% MET removal, while the UV/RHB–ZnO material achieved approximately 96.8% removal at a contaminant concentration of 10 mg $L^{-1}$ after 120 min of irradiation. Mineralization studies further revealed that, the zinc oxide-modified biochar system promoted more extensive degradation of organic intermediates compared with the silica-reinforced gelatin matrix. Kinetic evaluation demonstrated rapid degradation behavior for both materials, indicating effective contaminant decomposition under UV irradiation. Adsorption experiments confirmed that the silica-containing biopolymeric network possessed greater contaminant uptake capability than the zinc oxide-functionalized biochar structure. After 15 consecutive treatment cycles, the Gel–$SiO_2$ and RHB–ZnO composites retained 87% and 91% removal efficiency, respectively, demonstrating good operational stability and potential for reuse in pharmaceutical wastewater treatment. However, further studies using real wastewater and continuous-flow reactors are required to evaluate their performance in the presence of competing contaminants and under practical operating conditions.

**Keywords:** Vibrational spectroscopy; Adsorption; UV-irradiation; Diffraction analysis; Wastewater treatment.

## 1. INTRODUCTION

The continuous release of pharmaceutical compounds into aquatic environments has become a major environmental concern because of their persistence, biological activity, and incomplete removal by conventional wastewater treatment processes. Antibiotics are particularly problematic because their extensive use in human healthcare, veterinary medicine, and agriculture has resulted in their frequent occurrence in surface water, groundwater, and wastewater. Their persistence may also contribute to the development and spread of antimicrobial resistance, emphasizing the need for efficient and sustainable treatment technologies. Among pharmaceutical pollutants, metronidazole (MET) requires particular attention because effective removal from contaminated water remains challenging. Adsorption and photocatalysis are promising approaches for pharmaceutical wastewater treatment. Adsorption provides a simple and efficient means of concentrating pollutants on active material surfaces, whereas photocatalysis can promote their oxidative degradation through reactive species. Consequently, integrating suitable adsorptive properties with photocatalytic activity offers an attractive strategy for improving pharmaceutical removal. Sustainable polymeric

materials such as alginate, chitosan, cellulose, gelatin, and lignin have been investigated for adsorption and photocatalytic applications because of their biodegradability and abundant surface functional groups (Aminzai *et al.* 2023). Similarly, oxide-based materials have demonstrated high adsorption affinity and selectivity toward pharmaceutical contaminants (Mazurek *et al.* 2026; Harak *et al.* 2024).

Biochar and activated carbon derived from agricultural residues have been investigated as sustainable adsorbent materials for the removal of pollutants from aqueous systems (Rajesh *et al*. 2024). Rice husk-derived biochar (RHB) is a promising low-cost adsorbent because of its porous carbon structure, surface functional groups, silica-rich composition, and potential for regeneration (Lete *et al.* 2026). Structural investigations have confirmed that rice husk biochar consists predominantly of an amorphous carbon matrix containing residual silica-rich mineral phases, which can provide suitable sites for pollutant adsorption and catalyst immobilization (Demir and Bozkurt, 2026). However, adsorption alone primarily transfers pollutants from the aqueous phase to the solid phase rather than completely degrading them. Functionalization of biochar with semiconductor photocatalysts can therefore provide a combined adsorption–photocatalysis pathway for more effective contaminant removal.

ZnO is particularly attractive for such applications because of its semiconductor properties, photocatalytic activity, and ability to generate reactive oxygen species under irradiation. Its interaction with surface functional groups can also modify the surface chemistry of composite materials (Mathumitha *et al.* 2026). Biochar-supported metal oxide systems have already demonstrated improved pharmaceutical degradation because the porous biochar matrix enhances pollutant adsorption while facilitating charge transfer and reducing photocatalyst aggregation. For example, $ZnFe_2O_4$-supported rice husk biochar achieved effective tetracycline degradation (Fabris *et al.* 2026), while $Fe_3O_4$/rice husk biochar showed efficient ciprofloxacin removal and good recyclability (Toan *et al.* 2023). Rice husk biochar has been successfully utilized as a support material for photocatalysts, enhancing adsorption and photocatalytic degradation performance. Biochar–$TiO_2$ composites have shown efficient dye removal, demonstrating the suitability of rice husk-derived materials for sustainable water remediation (Malkari and Boddu, 2025). Rice husk-derived biochar-supported $CoFe_2O_4$ nanocomposite exhibits efficient adsorption–photocatalytic activity for pesticide degradation, achieving high removal of Lindane and DDE through hydroxyl radical-driven oxidation with stable reusability over multiple cycles (Rani and Shanker, 2024). SBA-15/$CeO_2$ mesoporous composites were successfully synthesized via precipitation–hydrothermal methods and extensively characterized by XRD, FTIR, SEM/EDS, TEM, and BET analyses, confirming uniform $CeO_2$ dispersion within the SBA-15 framework with enhanced surface area and reduced band gap for improved visible-light photocatalytic performance (Boonyuen *et al.* 2025). Similarly, rice husk biochar-supported photocatalysts have demonstrated high degradation performance and good reuse stability toward pharmaceutical pollutants (Yang *et al.* 2026; Rao *et al.* 2025). These findings indicate that ZnO-functionalized rice husk biochar (RHB–ZnO) may provide a sustainable platform combining pollutant adsorption with photocatalytic degradation.

In parallel, silica-based materials have attracted considerable interest as catalyst supports because of their high surface area, porous structure, hydrophilicity, chemical stability, and ability to disperse active photocatalytic phases. Mesoporous $TiO_2$–silica systems have demonstrated rapid pollutant degradation, highlighting the advantages of silica-supported photocatalysts (Alosaimi *et al.* 2021). Rice husk-derived mesoporous silica also provides an environmentally sustainable alternative to conventional silica sources (Shalaby *et al.* 2018). Recent silica-containing photocatalytic systems have further demonstrated efficient degradation of pharmaceutical contaminants and improved catalyst recovery and reuse (Al-Musawi *et al.* 2024; Moreira *et al.* 2025). Gelatin offers an additional sustainable matrix because of its biodegradability, film-forming ability, and functional groups capable of interacting with inorganic phases and organic pollutants. Incorporation of silica into gelatin can generate interconnected porous networks and strong organic–inorganic interfacial interactions. Mesoporous silica–gelatin hybrid materials have exhibited favorable surface area, mesoporosity, and structural integrity (Asiri *et al.* 2025). These characteristics suggest that silica-incorporated gelatin (Gel–$SiO_2$) could provide an effective adsorptive matrix while facilitating photocatalytic treatment under irradiation.

Despite these advances, most previous studies have focused on individual biochar-, metal oxide-, or silica-based systems and on pollutants such as tetracycline, ciprofloxacin, norfloxacin, and other organic contaminants. Comparatively less attention has been given to sustainable composite systems specifically designed for MET removal, particularly with respect to the combined assessment of adsorption, UV-assisted photocatalysis, regeneration, and repeated-cycle stability. Furthermore, a direct comparative evaluation of a ZnO-functionalized waste-derived biochar system and a silica-incorporated biodegradable polymer matrix remains limited. Addressing this gap is important for identifying sustainable materials capable of combining efficient pharmaceutical removal with practical reusability. Therefore, the novelty of the present study lies in the development and comparative investigation of two sustainable composite systems, ZnO-functionalized rice

husk biochar (RHB–ZnO) and silica-incorporated gelatin (Gel–$SiO_2$), for MET removal from aqueous media. The study aims to (i) synthesize and characterize RHB–ZnO and Gel–$SiO_2$ composites, (ii) compare their adsorption and UV-assisted photocatalytic performance through MET removal kinetics and degradation efficiency, and (iii) evaluate their regeneration capability and operational stability over repeated treatment cycles. The findings are expected to provide insight into the development of low-cost, environmentally sustainable, and reusable materials for the treatment of emerging pharmaceutical contaminants in water.

## 2. MATERIALS AND METHODOLOGY

### 2.1 Chemicals

Zinc nitrate hexahydrate [$Zn(NO_3)_2 \cdot 6H_2O$], absolute ethanol ($C_2H_6O$), and rice husk-derived biochar particles (2–5 mm) were employed for the preparation of the zinc oxide-modified biochar composite. Prior to composite fabrication, the biochar material was thoroughly washed with distilled water and dried in a hot-air oven at 105°C to remove impurities and residual moisture. Gelatin powder obtained from animal-derived collagen and high-purity silica nanoparticles (average particle size <100 nm) were utilized for the fabrication of the silica-reinforced biopolymeric composite. Sodium hydroxide (NaOH) solution was used to facilitate gel formation and improve the structural stability of the composite matrix. Metronidazole ($C_6H_9N_3O_3$, purity ≥99%) was selected as the model pharmaceutical contaminant for photocatalytic and adsorption degradation experiments. Representative aqueous solutions were prepared using deionized water. All reagents employed throughout the study were of analytical grade and used without purification.

### 2.2 Preparation of ZnO–rice Husk Biochar Composite

A zinc oxide precursor solution was prepared by dissolving 5 g of zinc nitrate hexahydrate [$Zn(NO_3)_2 \cdot 6H_2O$] in 50 mL of absolute ethanol under continuous magnetic stirring until a homogeneous solution was obtained (Alhuda and Mohammed, 2021). Subsequently, 1 mL of sodium hydroxide solution was added dropwise, followed by gradual addition of 250 mL of deionized water to promote hydrolysis and nucleation of zinc-based particles. The resulting suspension was continuously stirred until uniform dispersion was achieved. Predetermined quantities of rice husk-derived biochar were then introduced into the reaction medium and mixed for an additional 30 min to facilitate the deposition of zinc-containing species onto the porous carbon surface. The mixture was maintained in a thermostatically controlled water bath at 80°C for 5 h to ensure complete growth and attachment of the active phase. After cooling to ambient temperature, the obtained composite was repeatedly washed with distilled water to eliminate residual impurities, followed by oven drying at 80°C for 12 h. The dried material was thermally treated at 400°C for 2 h in a muffle furnace to obtain a zinc oxide-functionalized rice husk biochar composite suitable for photocatalytic applications (Wu *et al.* 2026). The NaOH solution had a concentration of 1.0 M and was added at 2.0 mL $min^{-1}$. For the selected formulation, 2.0 g of biochar was treated with 100 mL of precursor solution at a stirring speed of 500 rpm; after calcination, the composite yield was 2.8 g (70%).

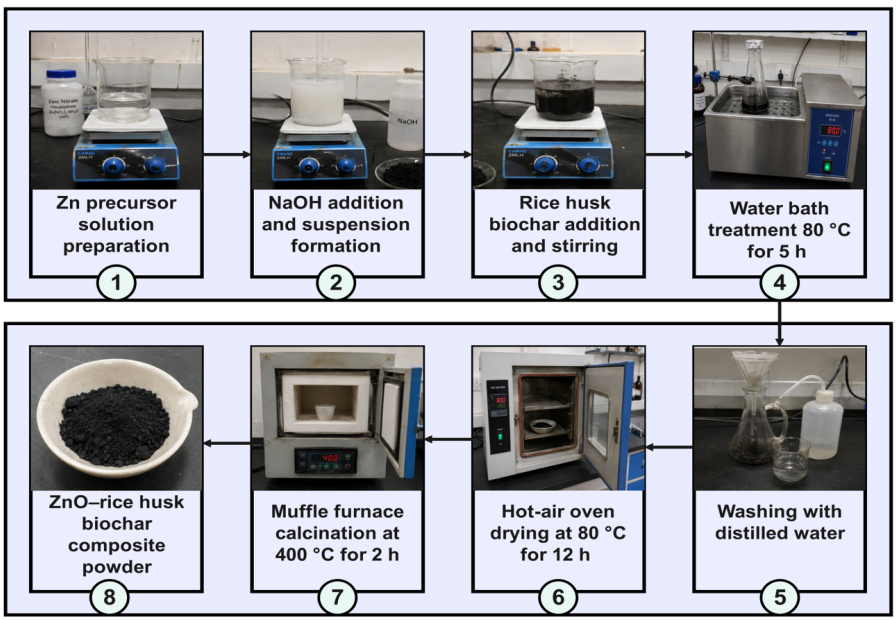


**Fig. 1: Experimental procedure for the preparation of ZnO–rice husk biochar composite powder**

## 2.3 Preparation of Silica Nanoparticles

Silica nanoparticles were synthesized by the sol–gel method with sodium silicate as the silica source. Initially, 10 g of sodium silicate was dissolved in 100 mL of distilled water under magnetic stirring to obtain a homogeneous solution (Palanimuthu *et al.* 2025). The dilute hydrochloric acid was added dropwise until the pH reached approximately 2, promoting the formation of a silica-rich gel. The resulting suspension was continuously stirred for 3 h at ambient temperature to ensure complete hydrolysis and condensation reactions. The formed gel were aged for 24 h to improve network development and structural stability. Thereafter, the precipitated material was repeatedly washed with distilled water to eliminate residual ions and reaction by-products. The purified product was separated by centrifugation and dried in a hot-air oven at 80°C. Finally, the dried powder was gently pulverized with an agate mortar and pestle to obtain fine silica nanoparticles suitable for composite fabrication and photocatalytic applications.

## 2.4 Preparation of Silica–gelatin Composite

Two grams of gelatin powder were dispersed in 100 mL of distilled water and heated at 60 °C under continuous magnetic stirring for 3 h until a clear, homogeneous solution was obtained. Subsequently, 0.50 g of synthesized silica nanoparticles was gradually added, corresponding to a silica-to-gelatin mass ratio of 1:4. The mixture was ultrasonicated at 40 kHz and 100 W for 30 min to ensure uniform silica dispersion. The resulting suspension was added dropwise at approximately 1 mL $min^{-1}$ to 50 mL of 0.5 M NaOH solution, producing composite beads with an average diameter of approximately 2.5 mm. The beads were maintained in the alkaline solution for 2 h to allow complete gelation and structural stabilization. They were subsequently washed with deionized water at 6 h intervals for a total of 12 h to remove residual chemicals and then dried in a hot-air oven at 70 °C until a constant mass was obtained. The final dry yield was 1.80 g, corresponding to approximately 72% of the initial dry mass. The resulting silica-reinforced gelatin composite was collected and used in the adsorption and UV-assisted MET-removal experiments.

## 2.5 Photocatalytic Reactor

Photocatalytic experiments were conducted in a quartz batch reactor with a total volume of 500 mL, working volume of 400 mL, internal diameter of 8 cm, and liquid depth of 10 cm. Two 16 W UVC lamps with a maximum emission wavelength of 254 nm were positioned 10 cm from the solution surface, providing an incident intensity of 1.2 mW $cm^{-2}$ as measured using an ILT2400 radiometer. The reactor was open and continuously stirred at 300 rpm; its temperature was maintained at 25 ± 1 °C using a circulating water bath.

## 2.6 Optimization of ZnO–rice Husk Biochar and Silica–gelatin Composite Synthesis

The proportion of zinc precursor solution to rice husk-derived biochar was optimized through a series of composite trials to obtain a uniformly coated photocatalytic composite. Initially, the precursor concentration was maintained at a fixed level while the quantity of biochar support was varied between 25 and 100 g (RZ-1 to RZ-3). Based on the extent of surface coverage and particle distribution observed during preliminary characterization, the most suitable biochar loading was selected for further optimization. The Gel–$SiO_2$ synthesis conditions were selected based on reported silica–gelatin sol–gel processing parameters. A formulation containing approximately 25 wt.% gelatin (1.6 g), 4.1 g $SiO_2$ derived from TEOS, and 0.6 g $SiO_2$ derived from GPTMS was considered suitable for stable hybrid-network formation. The precursors were mixed for 30 min at room temperature, followed by gelation for approximately 60–120 min and aging at 50 °C. These conditions facilitate TEOS hydrolysis and condensation and promote effective interaction between the silica and gelatin phases (Reyes-Peces *et al.* 2023). The RHB–ZnO formulations were compared based on ZnO surface coverage, particle-distribution uniformity, composite yield, and structural stability during washing. Based on these criteria, the formulation containing 2.0 g of rice-husk biochar and 100 mL of zinc precursor solution was selected because it produced uniform ZnO deposition and a final composite yield of 2.8 g.

**Table 1. Various combinations performed for the optimization of ZnO loading on rice husk biochar composite**

| Sample Codes | Zinc Precursor Solution Volume (mL) | Rice Husk Biochar Amount (g) | Estimated ZnO Loading (%) |
|---|---|---|---|
| RZ-1 | 5 | 25 | 0.54 |
| RZ-2 | 5 | 50 | 0.27 |
| RZ-3 | 5 | 100 | 0.14 |
| RZ-4 | 10 | 25 | 1.08 |
| RZ-5 | 15 | 25 | 1.61 |
| RZ-6 | 20 | 25 | 2.14 |

Similarly, different silica-to-gelatin ratios were investigated to optimize the preparation of the silica-reinforced biopolymeric composite. The optimization matrix and corresponding formulation conditions are

given below. In addition, the aqueous stability of fabricated composite beads was evaluated by periodically measuring their weight variation during prolonged immersion in deionized water. The Gel–$SiO_2$ formulations were evaluated according to bead formation, size uniformity, aqueous stability, material loss during washing, and dry yield. Based on these criteria, the formulation containing 2.0 g of gelatin and 0.50 g of silica nanoparticles (1:4 mass ratio) was selected because it produced uniform beads with an average diameter of approximately 2.5 mm, maintained its structural integrity during washing, and provided a final dry yield of 1.8 g.

## 2.7 Calculation for Theoretical ZnO Loading on Rice Husk Biochar Under Ideal Conditions, Assuming 100% Conversion and Deposition Efficiency – RZ-1

For RZ-1, 5 mL of zinc precursor solution was used for 25 g of rice husk biochar.

Precursor concentration = (5 g $Zn(NO_3)_2 \cdot 6H_2O$ in 50 mL ethanol)

Therefore, precursor present in 5 mL = (0.5 g $Zn(NO_3)_2 \cdot 6H_2O$)

Molecular weight of $Zn(NO_3)_2 \cdot 6H_2O$ = 297.49 g $mol^{-1}$

Weight of ZnO = 81.38 g $mol^{-1}$

Theoretical ZnO formed = 0.5 × 81.38 / 297.49 = 0.137 g

Estimated ZnO loading: = 0.137 / (25 + 0.137) × 100 = 0.54%

So, the theoretical ZnO loading for RZ-1 is 0.54%.

## 2.8 Adsorption Studies

Adsorption experiments were conducted in 250 mL Erlenmeyer flasks containing 100 mL of MET solution and 0.02 g of either ZnO-functionalized rice-husk biochar or silica-reinforced gelatin composite. The experiments were performed at initial MET concentrations of 0.1, 1, and 10 mg $L^{-1}$. The adsorbent dosage was therefore 0.20 g $L^{-1}$ and was selected to provide sufficient adsorbent–pollutant contact while minimizing material consumption. The initial solution pH was measured before each experiment and was not adjusted, allowing adsorption to be evaluated at the natural pH of the prepared MET solution. The flasks were agitated on an orbital shaker at 100 rpm and maintained at approximately 30 °C. Samples were collected at 30 min intervals until adsorption equilibrium was reached, and the residual MET concentration was determined using HPLC.

## 2.9 Photocatalytic and Reusability Studies

The photocatalytic efficiency of the zinc oxide-functionalized rice husk biochar composite and silica-reinforced gelatin composite was evaluated using metronidazole solutions at initial concentrations of 0.1, 1, and 10 mg $L^{-1}$. Experiments were carried out in batch reactors containing a predetermined amount of photocatalyst dispersed in the contaminant solution. Continuous mixing was maintained using a magnetic stirrer to ensure uniform suspension of catalyst particles and effective interaction among active sites and pollutant molecules. Ultraviolet irradiation was provided by two 16 W UVC lamps operating at a maximum wavelength of 254 nm. Similar UV-irradiated batch reactor systems have been successfully employed for the photocatalytic degradation of metronidazole using composite photocatalysts (Jerônimo *et al.* 2026).

The regeneration capability of the developed composites was assessed through repeated-use experiments. After each cycle, the composites were recovered using a stainless-steel mesh with an aperture size of 100 µm, washed three times with 50 mL of deionized water, and dried at 60 °C for 12 h before reuse. Recovery efficiency was determined gravimetrically as the recovered dry mass divided by the initial catalyst mass × 100. No fresh composite was added between cycles. After 15 cycles, the cumulative material loss was 4.8%, corresponding to an overall catalyst recovery of 95.2%. A total of 15 consecutive cycles were performed to analyse long-term stability and reusability of materials. All photocatalytic experiments were conducted under ambient laboratory conditions without external adjustment of pH or temperature. The reaction duration was maintained at 120 min, and aliquots were collected every 30 min for the determination of residual metronidazole concentration and degradation efficiency.

### 2.9.1 Control Experiments

Three control experiments were conducted under otherwise identical conditions: (i) MET with the composite in darkness to determine adsorption, (ii) MET under UV irradiation without a composite to determine direct photolysis, and (iii) MET without UV irradiation or composite to evaluate non-photochemical losses. After 120 min, the respective MET removals were 8%, 12%, and 3%, compared with 92% for the complete UV/composite system.

## 2.10 Analytical Techniques

Functional groups and chemical interactions within the silica-reinforced gelatin composite before and after treatment were investigated using a Fourier

transform infrared spectrometer (PerkinElmer, Akron, OH, USA) operating in attenuated total reflectance mode. FTIR spectra were recorded over 4000–400 $cm^{-1}$ at a resolution of 4 $cm^{-1}$ using 32 scans per sample.

The textural properties of rice husk biochar, silica nanoparticles, zinc oxide-functionalized rice husk biochar composite, and silica-reinforced gelatin composite were evaluated through nitrogen adsorption–desorption measurements at 77 K using a porosity analyzer and surface area (Micromeritics ASAP 2020). Specific surface area was determined by the Brunauer–Emmett–Teller technique, while pore size distribution was calculated by the Barrett–Joyner–Halenda method. Prior to analysis, the zinc oxide-modified biochar composite was degassed at 150°C, whereas the silica-reinforced gelatin composite was degassed at 100°C to remove adsorbed moisture and volatile species. BET measurements were conducted at 77 K after degassing RHB–ZnO at 150 °C and Gel–$SiO_2$ at 100 °C for 12 h; the BET fitting range was $P/P_0$ = 0.05–0.30.

The crystalline characteristics of the synthesized photocatalytic material were analyzed by X-ray diffractometer (Bruker) with Cu Kα radiation. XRD patterns were recorded over 2θ = 10–80° using Cu Kα radiation (λ = 1.5406 Å), a step size of 0.02°, a scanning rate of 1° $min^{-1}$, an operating voltage of 40 kV, and a current of 30 mA. The average crystallite size of the active phase was estimated from the most intense diffraction peaks by the Debye–Scherrer equation:

$$D = \frac{k\lambda}{\beta \cos\theta} \quad \dots (1)$$

Where λ represents incident X-ray radiation, k is the shape factor (0.9), θ corresponds to the Bragg diffraction angle (degrees), and β shows the full width at half maximum.

MET was quantified using an HPLC system equipped with a UV detector and a C18 column (250 mm × 4.6 mm, 5 µm particle size). The mobile phase consisted of acetonitrile and water (40:60, v/v) at 1.0 mL $min^{-1}$, with an injection volume of 20 µL and detection at 233 nm; the MET retention time was approximately 3.8 min. Calibration was performed over 0.5–50 mg $L^{-1}$ and showed linearity with $R^2$ = 0.999. The method exhibited an LOD of 0.1 mg $L^{-1}$, an LOQ of 0.3 mg $L^{-1}$, recovery of 98–102%, and intra- and interday relative standard deviations below 2%. Solution pH and temperature were monitored using calibrated digital probes. Residual organic carbon was measured using a Shimadzu TOC-L analyzer calibrated with potassium hydrogen phthalate standards over a concentration range of 0–100 mg $L^{-1}$.

## 2.11 Adsorption of MET

Amount of metronidazole adsorbed per unit mass of zinc oxide-functionalized rice husk biochar composite or silica-reinforced gelatin composite ($q_e$, mg $g^{-1}$) was calculated as

$$q_e = (C_0 - C_e)\frac{V}{W} \quad \dots (2)$$

$$q_e = \frac{q_{mL}K_L C_e}{1+K_L C_e} \quad \dots (3)$$

$$q_e = K_F C_e^{1/n_L} \quad \dots (4)$$

$$q_e = \frac{RT}{b_T}\ln(A_T C_e);\ B = \frac{RT}{b_T} \quad \dots (5)$$

$$\mathrm{n}\, q_e = \ln q_m - (K_{DR}\varepsilon^2);\ E\frac{1}{\sqrt{2K_{DR}}} \quad \dots (6)$$

$$\log(q_e - q_t) = \log q_e - \frac{k_1}{2.303}t \quad \dots (7)$$

$$\frac{t}{q_t} = \frac{1}{k_2 q_e^2} + \frac{1}{q_e}t \quad \dots (8)$$

The intraparticle diffusion behavior of metronidazole within the zinc oxide-functionalized rice husk biochar composite was evaluated by Weber–Morris diffusion model:

$$q_t = k_{id}t^{1/2} + c \quad \dots (9)$$

Where qt and qe denote the adsorption capacities of the developed composites (mg $g^{-1}$) at time t. Pseudo-first-order rate constant ($k_1$, $min^{-1}$), pseudo-second-order rate constant ($k_2$, g $mg^{-1}$ $min^{-1}$), and intraparticle diffusion coefficients (kid, g $mg^{-1}$ $min^{-0.5}$) were determined from corresponding linearized forms of Eqs. (6)–(8), respectively.

## 2.12 MET Elimination Rate

Efficiency of metronidazole degradation through the photocatalytic process was calculated as

$$\eta = \frac{C_0 - C_t}{C_0} \times 100 \quad \dots (10)$$

The metronidazole degradation rate constant ($k_1$) was determined using the Langmuir–Hinshelwood kinetic model:

$$\ln\frac{C_t}{C_0} = -K_1 t \quad \dots (11)$$

Where $C_0$ and $C_t$ show metronidazole concentration (mg $L^{-1}$) at the initial time and after 120 min of treatment.

## 2.13 Quality Assurance and Quality Control

All experiments were performed in triplicate, and results are reported as mean ± standard deviation. Procedural blanks, catalyst blanks, matrix-spiked samples, and calibration-verification standards were analyzed with each batch. Calibration was accepted when

$R^2 \geq 0.998$, and continuing calibration checks were required to remain within ±5% of the expected concentration. Sample recoveries ranged from 95% to 103%, while relative standard deviations remained below 3%. Glassware was cleaned using a detergent wash followed by deionized water rinsing and oven drying, and samples were filtered through 0.45-µm filters and analyzed within 24 h of collection.

## 3. RESULTS AND DISCUSSION

### 3.1 Characterization of ZnO–rice Husk Biochar and Silica–gelatin Composites

The photocatalytic performance of the zinc oxide-functionalized rice husk biochar composite was strongly influenced by crystallite size and surface distribution of the active phase. A reduction in crystallite size generally enhances the available reactive sites, thereby improving photocatalytic activity. An XRD pattern of the synthesized material exhibited diffraction peaks at 2θ values of 31.7°, 34.4°, 36.2°, 47.5°, 56.6°, 62.8°, 67.9°, 69.1°, and 76.9°, corresponding to the (100), (002), (101), (102), (110), (103), (112), (201), and (202) crystallographic planes of ZnO, respectively. This closely agree with the recently reported ZnO/biochar peaks at 31.8°, 34.4°, 36.2°, 47.5°, 56.6°, 62.9°, 68.0°, 69.1°, and 77.1°, confirming retention of the hexagonal wurtzite ZnO structure after incorporation into the biochar matrix (Tai *et al.* 2026). The average crystallite size was estimated by the Debye–Scherrer equation from the most intense diffraction peak. In addition, broad diffraction bands observed near 23° and 43° were attributed to the amorphous carbon structure of the rice husk-derived biochar. The diffraction profile of silica nanoparticles displayed a broad halo centered around 22°, indicating their predominantly amorphous nature. Similarly, the silica-reinforced gelatin composite exhibited a diffuse peak in the range of 20–22°, confirming the non-crystalline character of the biopolymeric matrix and successful incorporation of silica within the composite structure.

FTIR spectra of silica nanoparticles, gelatin, and the synthesized silica–gelatin composite Fig. 3 exhibited broad absorption bands at approximately 3440 $cm^{-1}$ (silica), 3400 $cm^{-1}$ (gelatin), and 3385 $cm^{-1}$ (silica–gelatin composite), corresponding to O–H and N–H vibrations. Absorption peaks observed near 2930 $cm^{-1}$ for gelatin and 2925 $cm^{-1}$ for the composite were C–H stretching vibrations. The characteristic bands located at 1652 $cm^{-1}$ and 1542 $cm^{-1}$ in gelatin, and 1645 $cm^{-1}$ and 1535 $cm^{-1}$ in the composite were assigned to amide I and amide II vibrations. These values closely agree with a recent silica-containing gelatin system, where characteristic gelatin bands were observed at 1638 and 1533 $cm^{-1}$ and silica-related vibrations occurred within 900–1250 $cm^{-1}$ (Prochon *et al.* 2025). The slight shifts observed in the present composite therefore support hydrogen bonding and interfacial interactions between silica and the gelatin matrix. The silica spectrum showed a band at 1630 $cm^{-1}$ associated with H–O–H bending of adsorbed water molecules. Characteristic silica-related absorption bands appeared at 1085 $cm^{-1}$ for silica and 1080 $cm^{-1}$ for the composite, corresponding to Si–O–Si asymmetric stretching vibrations. Additional bands at approximately 800 $cm^{-1}$ were attributed to Si–O–Si symmetric stretching vibrations, while an absorption band near 460 $cm^{-1}$ corresponded to Si–O bending vibrations. The presence of both amide and silica characteristic bands, along with slight shifts in peak positions, confirms the successful incorporation of silica into the gelatin matrix and indicates intermolecular interactions between the inorganic and biopolymeric phases.

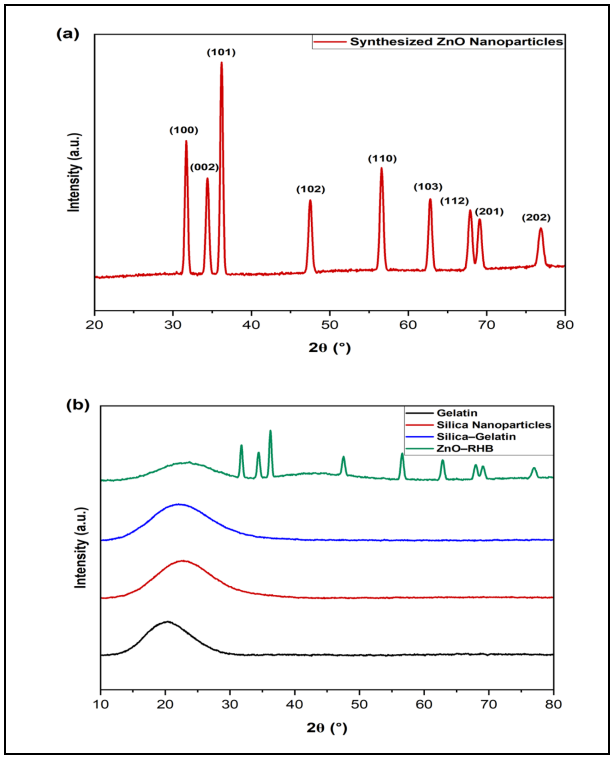


**Fig. 2: XRD of (a) synthesized ZnO nanoparticles and (b) gelatin, silica nanoparticles, silica–gelatin composite and ZnO-functionalized rice husk biochar composite**

The pore structure and specific surface area of rice husk biochar, zinc oxide-functionalized rice husk biochar, silica nanoparticles, and the silica-reinforced gelatin composite are summarized in Table 2. The incorporation of the active inorganic phase onto the porous carbon support resulted in a noticeable modification of the surface area and pore characteristics. The rise in surface area was attributed to the uniform distribution of fine particles within the porous framework, generating additional accessible adsorption sites. Adsorption–desorption isotherms of carbon-based materials [Fig. 4(a, b)] show Type IV BET characteristics with distinct hysteresis loops, confirming predominance

of mesoporous structures. Maximum nitrogen adsorption capacities reached 255 $cm^3 g^{-1}$ STP for RHB and 270 $cm^3 g^{-1}$ STP for ZnO–RHB at high relative pressures ($P/P_0 \approx 1.0$). The pore-size distribution indicated the presence of mesopores and larger interparticle pores, with most pores distributed within the 2–50 nm range. Previous studies on mesoporous silica–gelatin-supported metal oxide composites reported uniformly dispersed nanoparticles with an average particle size of approximately 26 nm, which contributed to the development of accessible surface area and porous characteristics (Ulfa and Lestari, 2025). Similarly, the adsorption–desorption profiles of silica nanoparticles and the silica-reinforced gelatin composite [Fig. 4(c, d)] also followed Type IV BET isotherms, indicating the existence of a porous network favorable for adsorption and photocatalytic applications. Although the nitrogen uptake increased from approximately 145 to 180 $cm^3 g^{-1}$ STP, the calculated BET surface areas of the silica nanoparticles and Gel–$SiO_2$ composite were 1.602 and 0.060 $m^2 g^{-1}$, respectively. This apparent inconsistency requires verification of the BET calculation, sample mass, degassing conditions, and units before a definitive interpretation of the textural changes can be made. Similar heterogeneous and porous morphologies have been reported for rice husk-derived biochars, where the preservation of surface area and pore structure after pyrolysis contributed to favorable adsorption characteristics and environmental remediation potential (Demir and Bozkurt, 2026).

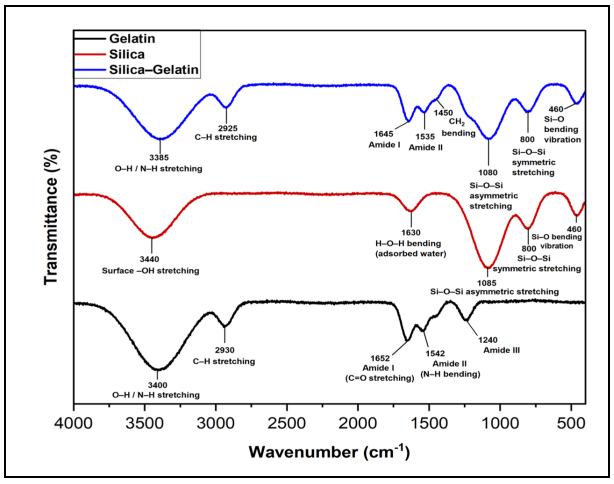


**Fig. 3: FTIR spectra of gelatin, silica nanoparticles, and synthesized silica–gelatin composite**

The BET surface area of the present RHB increased from 546.32 to 564.22 $m^2/g$ after ZnO functionalization, accompanied by an increase in total pore volume from 0.2978 to 0.3046 $cm^3/g$. A similar trend was recently reported for rice-husk-derived biochar, where ZnO–$Fe_3O_4$ functionalization increased the surface area from 218.5 to 486.3 $m^2/g$ and produced a pore volume of 0.412 $cm^3/g$ (El-Sawaf *et al.* 2027). The present RHB–ZnO exhibited a higher absolute surface area of 564.22 $m^2/g$, supporting the availability of abundant adsorption and photocatalytically active sites.

**Table 2. Pore structure and rice husk biochar and ZnO–rice husk biochar composite**

| Sample | Vmic ($cm^3 g^{-1}$) | Smic ($m^2 g^{-1}$) | Vt ($cm^3 g^{-1}$) | SBET ($m^2 g^{-1}$) |
|---|---|---|---|---|
| Rice husk biochar | 0.2429 | 464.18 | 0.2978 | 546.32 |
| ZnO-functionalized rice husk biochar | 0.2529 | 484.88 | 0.3046 | 564.22 |
| Silica nanoparticles | 0.0007 | 4.64 | 0.0410 | 1.602 |
| Silica-reinforced gelatin composite | 0.0003 | 0.07 | 0.0150 | 0.06 |

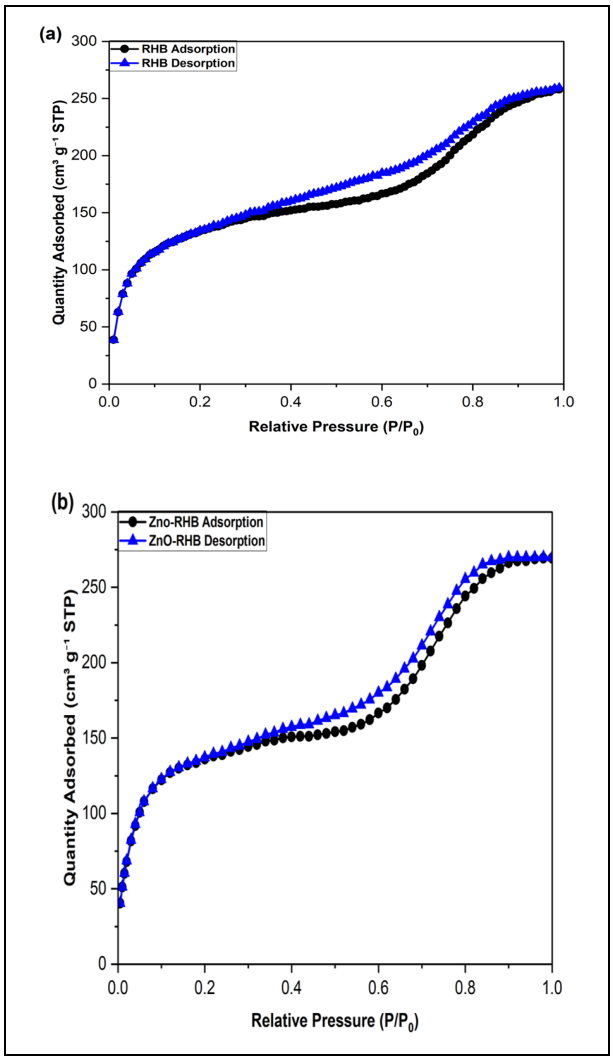

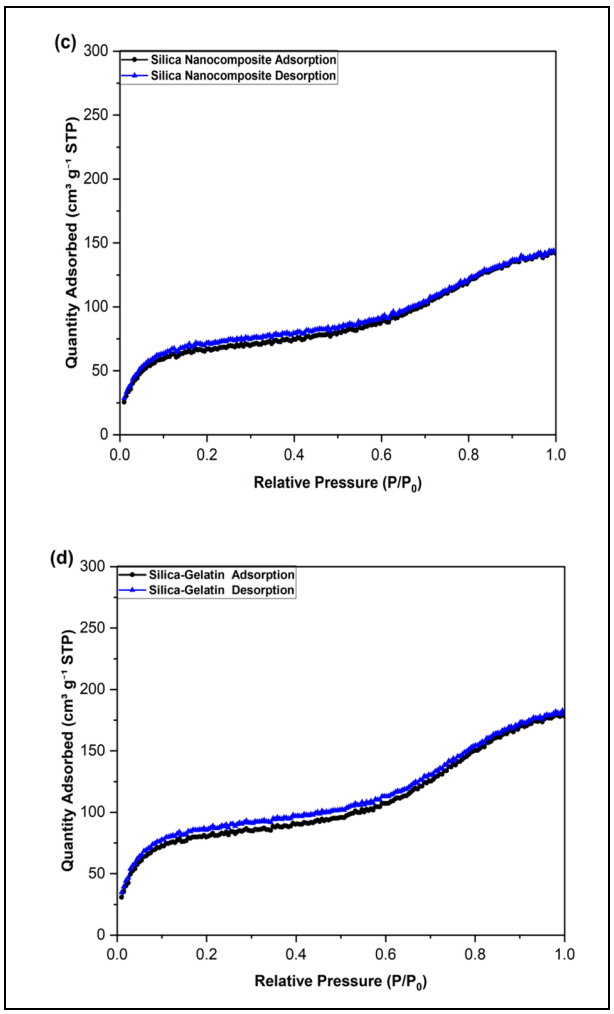


**Fig. 4: Nitrogen adsorption–desorption isotherms of (a) rice husk biochar, (b) ZnO-functionalized rice husk biochar, (c) silica nanoparticles and (d) silica–gelatin composite**

## 3.2 Adsorptive Removal of Metronidazole Using ZnO–rice Husk Biochar and Silica–gelatin Composites

The equilibrium was achieved after 1,440 min for the zinc oxide-functionalized rice husk biochar composite and 120 min for the silica-reinforced gelatin composite. The highest metronidazole adsorption rate and capacity constants of the developed materials were determined (Table 3). The adsorption performance of the zinc oxide-modified composite was compared with that of untreated rice husk biochar. Adsorption behavior of silica nanoparticles and the silica-reinforced gelatin composite suggested that removal efficiency was influenced not only by porosity and surface area but also by availability of surface functional groups. Furthermore, adsorption was governed by intermolecular interactions, including hydrogen bonding, electrostatic attraction, hydrophobic interactions, and surface complexation, between metronidazole molecules and the adsorbent surface.

The E by Eq. (6) was 40.11 kJ $mol^{-1}$, showing that chemisorption was the dominant mechanism governing metronidazole removal. The adsorption kinetics of the pseudo-first-order model for rice husk biochar, while silica nanoparticles, zinc oxide-functionalized rice husk biochar, and the silica-reinforced gelatin composite were better described by the pseudo second-order model, exhibiting high correlation coefficients ($r^2$ = 0.95–0.98). Furthermore, the adsorption rate was lower for the developed composites than for the individual materials, as indicated by the corresponding $k_2$ values (Table 4). The statistical analysis correlated experimental and predicted data using the Karl Pearson correlation coefficient.

## 3.3 Statistical Analysis

Adsorption-model performance was evaluated using the coefficient of determination ($R^2$) and residual-error analysis. The Freundlich model produced $R^2$ values of 0.99 for all four materials, compared with 0.75–0.98 for the Langmuir model and 0.73–0.86 for the Temkin model. These results indicate that the Freundlich model provided the most consistent representation of MET adsorption on the heterogeneous surfaces.

## 3.4 Photocatalytic Performance of ZnO–rice Husk Biochar and Silica–gelatin Composites

Photocatalytic investigations employing zinc oxide-functionalized rice husk biochar and silica-reinforced gelatin composite were performed at a catalyst dosage of 0.3 g $L^{-1}$ under 32 W ultraviolet irradiation. Furthermore, comparison between untreated rice husk biochar (2.5 g $L^{-1}$) and the zinc oxide-modified biochar composite (0.3 g $L^{-1}$) provided insight into the enhancement achieved through incorporation of the active photocatalytic phase. As shown in Table 6, high metronidazole removal efficiencies of 99.2% and 98.5% were achieved by the ZnO-functionalized rice husk biochar composite at 0.1 and 1 mg $L^{-1}$, respectively, while 96.8% removal was obtained at 10 mg $L^{-1}$. Similarly, the silica–gelatin composite exhibited removal efficiencies of 98.8%, 97.9%, and 94.5% at 0.1, 1, and 10 mg $L^{-1}$, despite the substantially lower catalyst dosage employed. As discussed earlier, adsorption performance was not solely controlled by surface area or porosity, and the contaminant concentration remained a key rate-determining factor. Other influential parameters included reactor operating mode, solution pH, and catalyst dosage. The initial MET concentration significantly influenced the removal efficiency of both composites. At a catalyst dosage of 0.3 g $L^{-1}$ and 32 W UV irradiation for 120 min, RHB–ZnO achieved 99.2%, 98.5%, and 96.8% MET removal at initial concentrations of 0.1, 1, and 10 mg $L^{-1}$, respectively, whereas Gel–$SiO_2$ achieved 98.8%, 97.9%, and 94.5%, respectively. The decrease in removal efficiency with increasing MET concentration is attributed to greater occupation of available active sites and increased competition for photogenerated reaction species. Although a fixed photocatalyst dosage of 0.3 g $L^{-1}$ provided high removal efficiency, further dosage optimization could identify the optimum balance between available active sites and UV-light penetration. Similarly, solution pH can modify both catalyst surface charge and MET speciation; therefore, systematic pH optimization is recommended for further investigation.

**Table 3. Adsorption isotherm calculated for pristine and composite materials**

| Composite | MET Working | Isotherm Data | | | | | | | | |
|---|---|---|---|---|---|---|---|---|---|---|
| | | Langmuir Isotherm | | | Freundlich Isotherm | | | Temkin Isotherm | | |
| | | $q_{mL}$ (mgg-1) | $K_L$ (Lmg-1) | $r^2$ | $K_F$ (mgg-1) | 1/n | $r^2$ | $A_r$(Lg-1) | B (Jmol-1) | $r^2$ |
| ZnO-functionalized rice husk biochar | 0.1, 1, and 10 | 1.41 | 0.64 | 0.98 | 0.54 | 0.66 | 0.99 | 0.33 | 2.94 | 0.86 |
| Rice husk biochar | 0.1, 1, and 10 | 3.17 | 0.07 | 0.90 | 1.15 | 0.13 | 0.95 | 9.37 | 0.39 | 0.73 |
| Silica-reinforced gelatin composite | 0.1, 1, and 10 | 1.22 | 0.42 | 0.93 | 10.8 | 0.59 | 0.99 | 0.59 | 5.22 | 0.83 |
| Silica nanoparticles | 0.1, 1, and 10 | 2.14 | 0.03 | 0.75 | 19.7 | 0.93 | 0.99 | 0.03 | 0.48 | 0.83 |

**Table 4. Parameters for pristine and composite materials**

| Composite | MET Range | $k_1$ | $q_e$ | $r^2$ | $k_2$ | $q_e$ | $r^2$ | Ki | C | $r^2$ |
|---|---|---|---|---|---|---|---|---|---|---|
| ZnO-functionalized rice husk biochar | 10 | 0.008 | 2.47 | 0.94 | 0.007 | 1.82 | 0.98 | 0.04 | 0.36 | 0.87 |
| Rice husk biochar | 15 | 0.011 | 0.67 | 0.98 | 0.062 | 1.12 | 0.93 | 0.07 | 0.30 | 0.64 |
| Silica-reinforced gelatin composite | 10 | 0.214 | 1.02 | 0.84 | 0.009 | 1.05 | 0.97 | 0.03 | 0.15 | 0.64 |
| Silica nanoparticles | 10 | 0.100 | 0.94 | 0.69 | 0.145 | 0.47 | 0.95 | 0.04 | 0.03 | 0.97 |

**Table 5. Photocatalytic efficiency of ZnO–rice husk biochar and silica–gelatin composites different initial MET concentrations at 120 min reaction time and 32 W UV power**

| Type of System | Catalyst Dosage | MET Removal (%) | | | MET Removal Rate ($min^{-1}$) | | | TOC Reduction After 120 Min (%) | | |
|---|---|---|---|---|---|---|---|---|---|---|
| | | 0.1 | 1 | 10 | 0.1 | 1 | 10 | 0.1 | 1 | 10 |
| ZnO-functionalized rice husk biochar | 0.3 | 99.2 | 98.5 | 96.8 | 0.031 | 0.028 | 0.021 | 80.1 | 78.9 | 76.4 |
| Rice husk biochar | 2.5 | 95.4 | 92.7 | 80.8 | 0.018 | 0.014 | 0.010 | 73.5 | 71.2 | 60.8 |
| Silica-reinforced gelatin composite | 0.3 | 98.8 | 97.9 | 94.5 | 0.029 | 0.025 | 0.019 | 76.8 | 74.9 | 71.8 |

Control experiments produced 8% MET removal by dark adsorption, 12% by direct photolysis, and 3% without UV irradiation or composite, compared with 92% for the combined UV/composite system after 120 min. These results support a synergistic contribution from adsorption and UV-assisted degradation; however, the involvement of individual reactive species requires confirmation through radical-scavenging or electron-spin-resonance experiments. The reactions associated with photocatalytic oxidation during contaminant degradation are presented in Eqs. (12)–(15). Upon ultraviolet irradiation of the zinc oxide-functionalized rice husk biochar composite, electrons in the valence band absorb sufficient energy and are promoted to the conduction band, resulting in the generation of electron–hole pairs, as given in eqn (12)

$$ZnO/RHB+h\nu \rightarrow eCB^{-}+hVB^{+} \quad \dots (12)$$

Conversely, water molecules react with the generated holes to form hydroxyl radicals and protons, as given in eqn (13)

$$H_2O+hVB^{+} \rightarrow OH+H^{+} \quad \dots (13)$$

$$O_2+eCB^{-} \rightarrow O_2^{-} \quad \dots (14)$$

Subsequently, metronidazole molecules react with hydroxyl and superoxide radicals and are mineralized as water and carbon dioxide, as given in eqn (15)

$$MET+OH/O_2^{-} \rightarrow \text{degradation products} \rightarrow CO_2+H_2O \quad \dots (15)$$

The metronidazole removal profiles obtained from photocatalysis and adsorption using the developed composites were presented in Fig. 5. Elimination curves indicate that a larger fraction of metronidazole was removed through adsorption by the silica-reinforced gelatin composite compared with the zinc oxide-functionalized rice husk biochar system. Under UV irradiation, both composites exhibited rapid metronidazole degradation and achieved high removal efficiencies within 120 min, particularly at lower initial concentrations. However, adsorption alone resulted in

comparatively lower removal efficiencies, especially at higher metronidazole concentrations. Furthermore, at lower initial concentrations, the zinc oxide-functionalized rice husk biochar composite demonstrated superior photocatalytic performance relative to the silica-reinforced gelatin composite, which was attributed to the photocatalytic activity of ZnO combined with the adsorption capability of the biochar support.

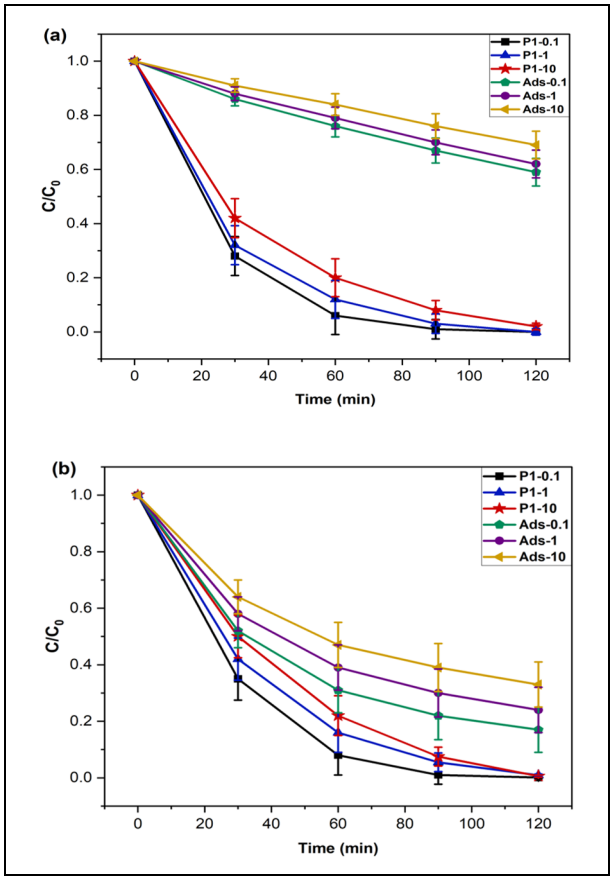


**Fig. 5: Metronidazole removal profiles obtained by photocatalysis and adsorption using (a) ZnO-functionalized rice husk biochar and (b) silica–gelatin composite at different initial metronidazole concentrations**

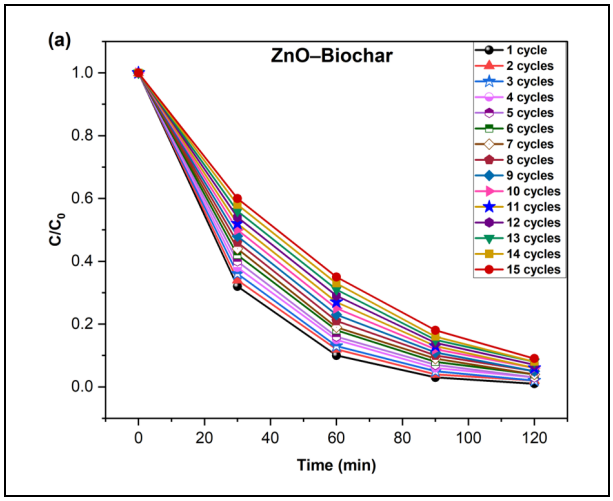


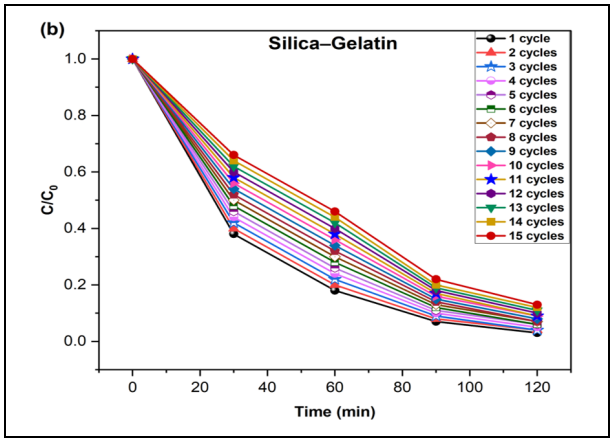


**Fig. 6: Reusability performance of (a) ZnO-functionalized rice husk biochar and (b) silica–gelatin composite during fifteen consecutive metronidazole degradation cycles under UV irradiation**

Reusability assessment was performed by repeating the photocatalytic degradation experiment using the developed composites over 15 consecutive cycles (P1–P15), and corresponding elimination profiles are presented in Fig. 6. The photocatalytic efficiency of the zinc oxide-functionalized rice husk biochar composite gradually decreased from approximately 98% in the first cycle (P1) to about 91% in the fifteenth cycle (P15). A noticeable reduction in metronidazole removal was observed after repeated usage, which can be attributed to mechanical abrasion during continuous stirring and partial loss of the active ZnO phase from the biochar surface. Similarly, the silica-reinforced gelatin composite exhibited a gradual decline in removal efficiency with increasing cycle number; however, it retained high photocatalytic activity throughout the 15-cycle evaluation period. The relatively small reduction in performance demonstrates the good structural stability and reusability of both developed composites for repeated metronidazole treatment. Comparable reusability behavior has been reported for rice husk biochar-supported $Cu/Cu_2O/BC$ photocatalysts, which retained 78.41% of their degradation efficiency after five consecutive cycles. The higher retention observed in the present study after 15 cycles further demonstrates the excellent stability of the developed composite system (Du *et al.* 2024). The photocatalytic performance of the developed composites was comparable with recently reported MET degradation systems. In a prior study, the authors achieved 98.5% degradation of 25 mg $L^{-1}$ MET within 90 min using an $\alpha$-$Fe_2O_3$/g-$C_3N_4$/Fe-MOF photocatalyst under sunlight irradiation (Bhuyan and Ahmaruzzaman, 2024) and 94.3% degradation of 10 mg $L^{-1}$ MET within 180 min using 0.5 mol% Nd–ZnO (Zhang et al., 2026). In comparison, the present study achieved 96.8% MET removal using RHB–ZnO and 94.5% using Gel–$SiO_2$ at 10 mg $L^{-1}$ within 120 min under UV irradiation. These results demonstrate that the developed sustainable composites provide competitive MET removal performance while utilizing low-cost rice husk biochar and gelatin-based supporting materials.

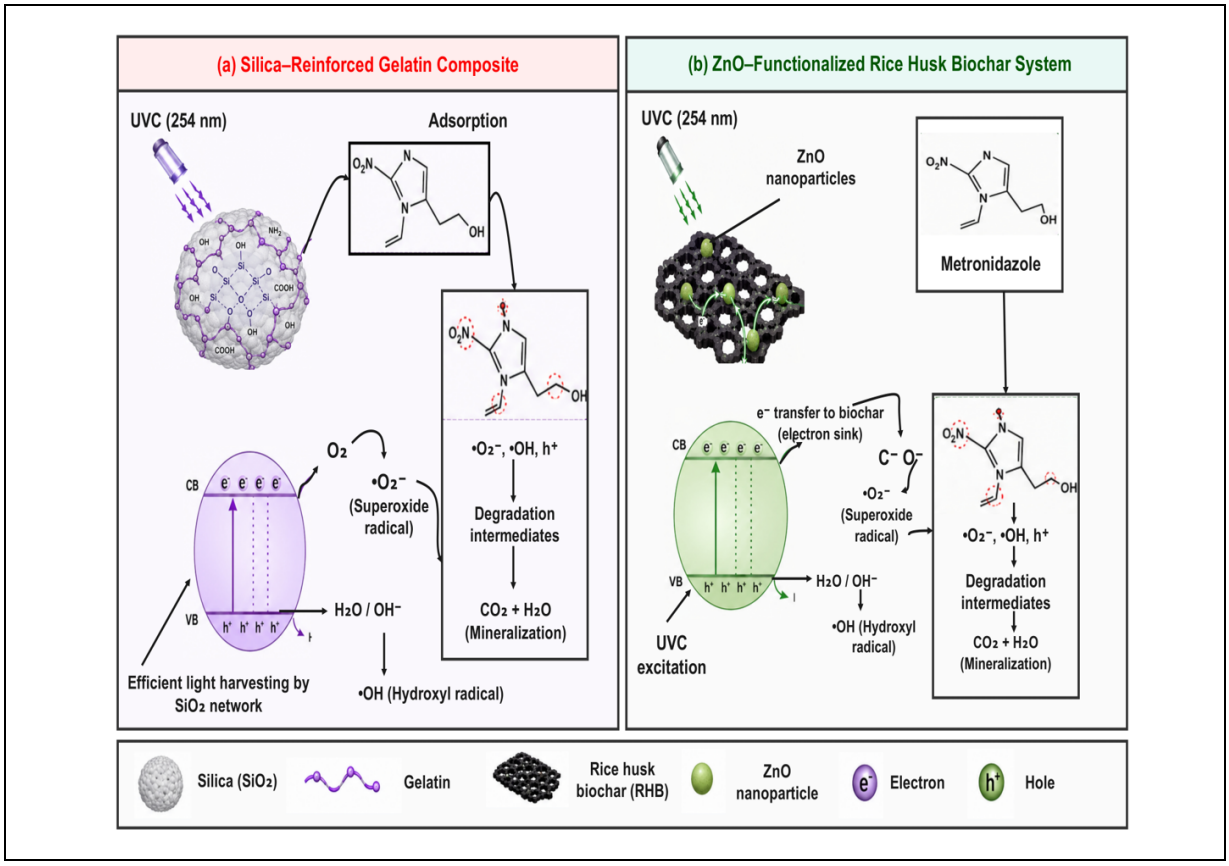


**Fig. 7: Proposed mechanism for metronidazole degradation using silica–reinforced gelatin and ZnO–functionalized rice husk biochar composites under UVC irradiation**

## 4. CONCLUSIONS

The zinc oxide-functionalized rice husk biochar composite and silica-reinforced gelatin composite were successfully synthesized and characterized in terms of crystal structure, pore characteristics, specific surface area, and surface functional groups. Prepared materials were subsequently evaluated for the adsorption and ultraviolet-assisted removal of metronidazole. Both developed composites exhibited substantially higher metronidazole elimination under UV irradiation than under adsorption alone, demonstrating the beneficial role of light-assisted degradation. The adsorption behavior of rice husk biochar followed pseudo-first-order kinetics, suggesting a predominantly physical adsorption mechanism, whereas the zinc oxide-functionalized rice husk biochar and silica-reinforced gelatin composite were better described by pseudo-second-order kinetics, indicating the contribution of chemisorption processes. The Freundlich isotherm model provided the best fit to equilibrium data, confirming the heterogeneous nature of adsorption on the developed materials. Reusability experiments demonstrated good operational stability for both composites over 15 consecutive treatment cycles. The silica-reinforced gelatin composite retained approximately 87% removal efficiency after the fifteenth cycle, while the zinc oxide-functionalized rice husk biochar composite maintained approximately 91% removal efficiency. Although the ZnO-modified biochar exhibited slightly greater long-term stability, the silica-reinforced gelatin composite showed superior adsorption-assisted metronidazole removal. Overall, both materials demonstrated promising potential for sustainable pharmaceutical wastewater treatment, with the silica-reinforced gelatin composite serving primarily as an efficient adsorbent and the zinc oxide-functionalized rice husk biochar providing enhanced photocatalytic degradation capability.

## FUNDING

This research received no specific grant from any funding agency in the public, commercial, or not-for-profit sectors.

## CONFLICTS OF INTEREST

The authors declare that there is no conflict of interest.

## COPYRIGHT

This article is an open-access article distributed under the terms and conditions of the Creative Commons

Attribution (CC BY) license (http://creativecommons.org/licenses/by/4.0/).

## REFERENCES


Alhuda, M. N. N. and Mohammed, M. A., Preparation of ZincOxide Nanoparticles by UV-Irradiation Method in Two Different Media, *J. Phy. Conf. Series*, 2114(1), 012079(2021). https://doi.org/10.1088/1742-6596/2114/1/012079

Al-Musawi, T. J., Bahrami, P. P., Rahimpoor, R., Mengelizadeh, N. and Balarak, D., Enhanced photocatalytic degradation of ciprofloxacin antibiotics using $Fe_3O_4$-$SiO_2$-EN@Zn-Al layered double hydroxide nanocomposites under the COVID-19 pandemic, *Res. Eng.*, 24, 103396(2024). https://doi.org/10.1016/j.rineng.2024.103396

Alosaimi, E. H., Alsohaimi, I. H., Dahan, T. E., Chen, Q., Younes, A. A., El-Gammal, B. and Melhi, S., Photocatalytic Degradation of Methylene Blue and Antibacterial Activity of Mesoporous $TiO_2$-SBA-15 Nanocomposite Based on Rice Husk, *Adsorp. Sci. Technol.*, 2021, 9290644(2021). https://doi.org/10.1155/2021/9290644

Aminzai, M. T., Azizi, N., Nural, Y. and Yabalak, E., A Review on Recent Advances in Polymer-Assisted Green and Sustainable Technology for Remediation of Pharmaceuticals from Water and Wastewater, *Water, Air, Soil Pollut.*, 234(11), 681(2023). https://doi.org/10.1007/s11270-023-06698-7

Asiri, M., Sead, F. F., Mayani, S. V, Menon, S. V, Thakur, R., Ray, S., Khalaf, R. M., Alsaffar, M. F., Mengelizadeh, N. and Balarak, D., Enhanced photocatalytic degradation of penicillin G using magnetic silica doped ZnAl- layered double hydroxides, *Sci. Rep.*, 15(1), 33110(2025). https://doi.org/10.1038/s41598-025-17327-0

Bhuyan, A. and Ahmaruzzaman, M., Ternary 3D/2D/3D direct dual Z-scheme MOF-on-MOF-derived α-$Fe_2O_3$/g-$C_3N_4$/Fe-MOF photocatalyst for boosted sunlight-driven removal of metronidazole: effect of coexisting ions, mechanistic insights, and water matrices, *Environ. Sci. Nano*, 11(12), 4805–4829 (2024). https://doi.org/10.1039/d4en00610k

Boonyuen, S., Smith, S. M., Luengnaruemitchai, A., Nakorn, P. N., Tangjaideborisu, Y. and Shanmugam, P., Amplified photocatalytic decay of organic dyes and antibiotic pollutants using hexagonal honeycomb mesoporous silica (SBA-15)/$CeO_2$ nanocomposites under visible-light exposure, *Inorg. Chem. Commun.*, 173, 113862(2025). https://doi.org/10.1016/j.inoche.2024.113862

Demir, Z. and Bozkurt, P. A., Co-pyrolysis of agricultural biomass for potentially functional biochar: combined influence of both feedstocks and structural characterization, *Sci. Rep.*, 16(1), 10947(2026). https://doi.org/10.1038/s41598-026-45350-2

Du, G., Ding, Y., Li, C., Zhang, L., Li, J., Li, M., Zhu, W. and He, C., Preparation of Cu/$Cu_2O$/BC and Its Performance in Adsorption–Photocatalytic Degradation of Methyl Orange in Water, *Mater.*, 17(17), 4306(2024). https://doi.org/10.3390/ma17174306

El-Sawaf, A. K., Nassar, A. A., Mohamed, M. A., Taha, A. and Mubarak, M. F., Circular valorization of rice husk waste into a magnetic ZnO–$Fe_3O_4$/Biochar multifunctional composite for sustainable remediation of pharmaceutical-contaminated water, *Biomass Bioenergy*, 216, 109710(2027). https://doi.org/10.1016/j.biombioe.2026.109710

Fabris, L. C., Ferreira, P. F. A. C., Machado, F. M., Swarowsky, A., Foletto, E. L., Souza, D. M., Carissimi, E. and Leichtweis, J., Rice husk waste biochar as a photocatalyst support for use in the degradation of organic pollutants, *Chem. Eng. Sci.*, 325, 123497(2026). https://doi.org/10.1016/j.ces.2026.123497

Harak, S. S., Krishnaveni, K., Karthick, K., Chinnarasu, K., Venkata, H. P. P., Tonk, A. and Mayakannan, S., Experimental Study on the Mechanical Properties of Hybrid Areca and Abaca Fiber Reinforced Polymer Composites, *J. Environ. Nanotechnol.*, 13(4), 92–101 (2024). https://doi.org/10.13074/jent.2024.12.244977

Jerônimo, A. G., Amorim, K., Albuquerque, W., Trigueiro, P., Romaguera-Barcelay, Y., Feitosa, R. P., Orta, M. D. M., Osajima, J. A. and Peña-Garcia, R. R., Rice husk ash–supported CdS composites for efficient photocatalytic degradation of metronidazole with minimized phytotoxicity, *J. Phy. Chem. Sol.*, 213, 113550(2026). https://doi.org/10.1016/j.jpcs.2026.113550

Lete, A., Navarro-Gil, Á., Millera, Á., Fonts, I., Ceamanos, J., Gil-Lalaguna, N. and Gea, G., Rice husk pristine biochar for dynamic gas-phase $NH_3$ adsorption: impact of pyrolysis temperature and mechanism, *Chem. Eng. Sci.*, 334, 124313 (2026). https://doi.org/10.1016/j.ces.2026.124313

Malkari, K. R. and Boddu, S., Advanced photocatalysis with biochar-$TiO_2$ composite for efficient oxidation of Congo red dye, *Environ. Monitor. Assess.*, 197(7), 831 (2025). https://doi.org/10.1007/s10661-025-14290-1

Mathumitha, S., Balamurali, M., Jeganathan, M. and Jeganathan, S., Multi-spectroscopic investigation of ZnO nanoparticle-induced biomolecular alterations in Saccharomyces cerevisiae, *Spectrochimica Acta - Part A: Mol. Biomol. Spectros.*, 359, 127970(2026). https://doi.org/10.1016/j.saa.2026.127970

Mazurek, K., Ciesielczyk, F. and Siwińska-Ciesielczyk, K., Adsorptive elimination of antibiotics from contaminated water utilising customised zirconia: material synthesis, characterisation, and efficiency in tetracycline and ampicillin removal, *J. Environ. Manage.*, 401, 128795 (2026). https://doi.org/10.1016/j.jenvman.2026.128795

Moreira, F. S., Trindade, B. B., Vale, M., Oliveira, M. C., Al Mohtar, A. and Marques, A. C., MICROSCAFS® for minocycline elimination from water and real wastewater: Porosity and $TiO_2$ nanoparticles effect, *Chem. Eng. J.,* 504, 158771(2025). https://doi.org/10.1016/j.cej.2024.158771

Palanimuthu, V., Anukeerthana, S., Periakaruppan, R., Priyanka, G. and Sasthri, G., Eco-friendly approach for synthesis of silica nanoparticles using extract of Ulva fasciata and an evaluation of its potential applications, *Biomass Convers. Biorefine.*, 15(23), 30329–30341 (2025). https://doi.org/10.1007/s13399-024-06235-4

Prochon, M., Dzeikala, O., Szczepanik, S. and Sędzikowska, N., Biodegradable Gel Blends with Enhanced Sensing Capabilities: $SIO_2$-Based Innovations for Sustainable and Eco-Friendly Packaging, *Chem. Europ. J.,* 31(32), e202403335(2025). https://doi.org/10.1002/chem.202403335

Rajesh, Y., Neha, G., Jai, S., Anil, K. T., Gole, S., Pragati, N. and Ganesh, D., Evaluation of Activated Biochar from Sustainable Sterculia foetida Shells for the Removal of AB 158 Dye, *J. Environ. Nanotechnol*., 13(2), 248-255(2024). https://doi.org/10.13074/jent.2024.06.242607

Rani, M. and Shanker, U., Green construction of biochar@$NiFe_2O_4$ nanocomposite for highly efficient photocatalytic remediation of pesticides from agriculture wastewater, *Chemosphere*, 352, 141337 (2024). https://doi.org/10.1016/j.chemosphere.2024.141337

Rao, D. P., Krishnasamy, V. D., Selvaraju, M., Sundramurthy, V. P., Kandavalli, S. R., Chitra, M. S., Sivasamy, N. and Thirumoorthy, P., Adsorptive removal of cadmium from electroplating wastewater using hybrid composite of thiol-grafted seed gum of Tamarindus indica and Teff hay biocarbon, *Zeitschrift Fur Physikalische Chemie*, 239(5), 633–654(2025). https://doi.org/10.1515/zpch-2024-0715

Reyes-Peces, M. V, Fernández-Montesinos, R., Mesa-Díaz, M. D. M., Vilches-Pérez, J. I., Cárdenas-Leal, J. L., de la Rosa-Fox, N., Salido, M. and Piñero, M., Structure-Related Mechanical Properties and Bioactivity of Silica–Gelatin Hybrid Aerogels for Bone Regeneration, *Gels*, 9(1), 67(2023). https://doi.org/10.3390/gels9010067

Shalaby, N. H., Elsalamony, R. A. and El Naggar, A. M. A., Mesoporous waste-extracted $SiO_2$-$Al_2O_3$-supported Ni and Ni-$H_3PW_{12}O_{40}$ nano-catalysts for photo-degradation of methyl orange dye under UV irradiation, *New J. Chem.*, 42(11), 9177–9186 (2018). https://doi.org/10.1039/c8nj01479e

Tai, J. W., Pang, Y. L., Chen, W.-H., Chih, Y.-K., Lim, S. and Chong, W. C., Sonocatalytic Degradation of Malachite Green Using a Sustainable ZnO/Biochar Composite Derived from Phytoremediated Plant Residue: Process Optimisation via Response Surface Methodology, *Catal.*, 16(4), 363(2026). https://doi.org/10.3390/catal16040363

Toan, T. Q., Mai, N. T., Trang, H. M., Van, H. P. and Van, T. D., Ultrasonic-assisted synthesis of magnetic recyclable $Fe_3O_4$/rice husk biochar based photocatalysts for ciprofloxacin photodegradation in aqueous solution, *RSC Adv.*, 13(16), 11171–11181 (2023). https://doi.org/10.1039/d3ra00178d

Ulfa, M. and Lestari, S., Design of Bi-and Tri-metal Oxide Photocatalysts via Gelatin-Directed Mesoporous Silica Hard Templating for Advanced Dye Degradation, *Bulletin Chem. React. Eng. Catal.*, 20(4), 661–671 (2025). https://doi.org/10.9767/bcrec.20460

Wu, B., Chen, Q., Islam, M. A. and Eljamal, O., Optimal synthesis of rice husk–derived biochar for Cr (VI) removal: Mechanistic interpretation based on pH evolution in biochar–nZVI systems, *J. Water Process Eng.*, 87, 110025(2026). https://doi.org/10.1016/j.jwpe.2026.110025

Yang, X., Zhao, J., Zhang, E., Jiang, B., Zhao, S., Luo, T., Sun, P., Yang, S., Han, Y., Wang, L., Zeng, F., Ding, C. and Gao, B., One-step calcination synthesis of rice husk biochar-doped g-$C_3N_4$ for efficient photodegradation of norfloxacin, *J. Hazard. Mater. Adv.*, 22, 101252 (2026). https://doi.org/10.1016/j.hazadv.2026.101252

Zhang, Q., Sa, G. and Xu, A., Nd-ZnO Catalysts for Photocatalytic Degradation of Metronidazole, *Chem. Select*, 11(25), e73736 (2026). https://doi.org/10.1002/slct.73736